

Supplementary material

Nanoscopy with more than a hundred thousand ‘doughnuts’

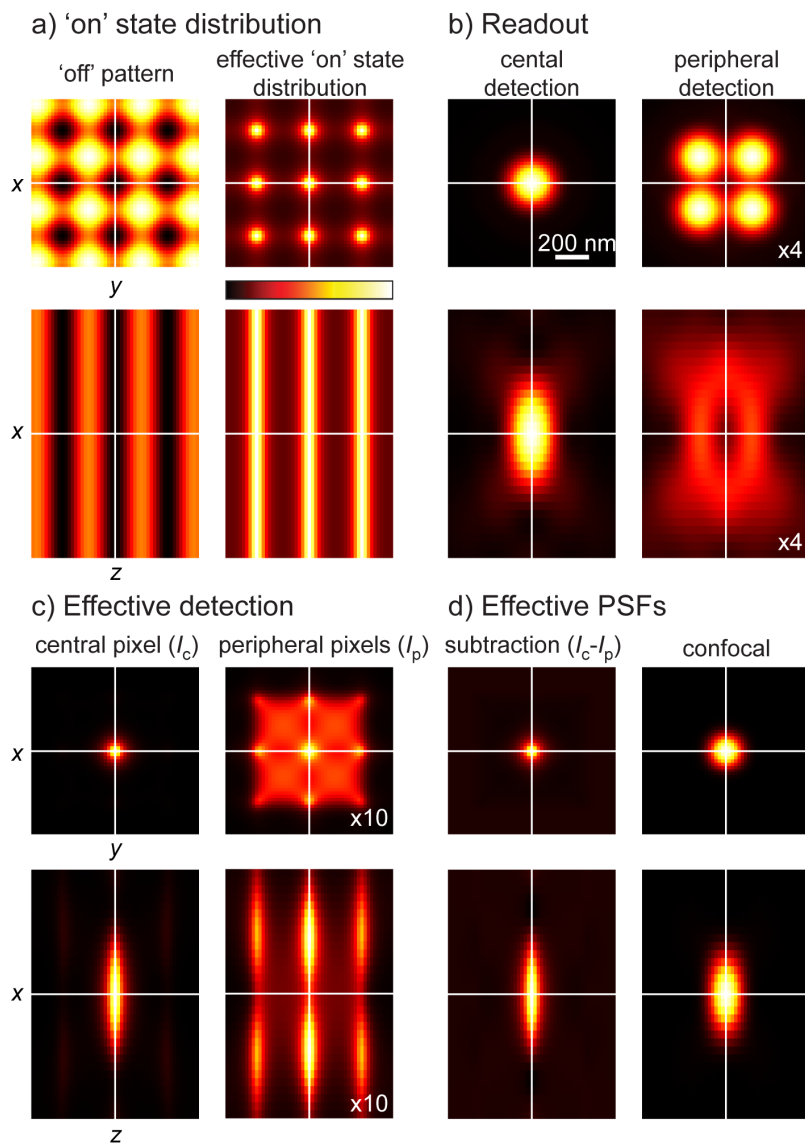
Andriy Chmyrov¹, Jan Keller¹, Tim Grotjohann¹, Michael Ratz¹, Elisa d’Este¹, Stefan Jakobs^{1,2}, Christian Eggeling¹ & Stefan W. Hell¹

¹Department of NanoBiophotonics, Max Planck Institute for Biophysical Chemistry, Göttingen, ²Department of Neurology, University of Göttingen, Germany

Correspondence should be addressed to SWH (shell@gwdg.de)

Section	Page
Supplementary Figures	
Supplementary Figure 1: Calculation of the 3D PSF of the microscope	2
Supplementary Figure 2: Calculation and measurement of the axial response of the microscope	3
Supplementary Figure 3: Full image of a section depicted in Fig. 2 c-d	4
Supplementary Figure 4: Spectral properties of rsEGFP(N205S)	5
Supplementary Figure 5: rsEGFP(N205S) is a monomer	6
Supplementary Figure 6: Maturation of rsEGFP(N205S) at 37 °C	7
Supplementary Figure 7: Expression of rsEGFP(N205S) fusion proteins in living mammalian cells	8
Supplementary Figure 8: Switching kinetics and brightness of rsEGFP(N205S)	9
Supplementary Figure 9: Fast parallelized RESOLFT imaging with 120 µm x 100 µm field of view	10
Supplementary Figure 10: Fast parallelized RESOLFT imaging with 50 µm x 50 µm field of view	11
Supplementary Figure 11: Off-switching (deactivation) pattern in parallelized RESOLFT	12
Supplementary Figure 12: Detailed diagram of the parallelized RESOLFT microscope	13
Supplementary Notes	
Supplementary Note 1: Lateral on-state spatial distribution	14
Supplementary Note 2: Optical sectioning capability of the parallelized microscope	15
Supplementary Note 3: Flat field correction of the sCMOS camera	16

Supplementary Figure 1: Calculation of the 3D PSF of the microscope



(a) Effective on-state distribution which is essentially determined by the off-switching pattern. The I/I_s is chosen to yield an 80 nm width of the on-state peaks. The pattern and the distribution are shown as colored intensity maps in xy (first row) and xz (second row), normalized to [0,1].

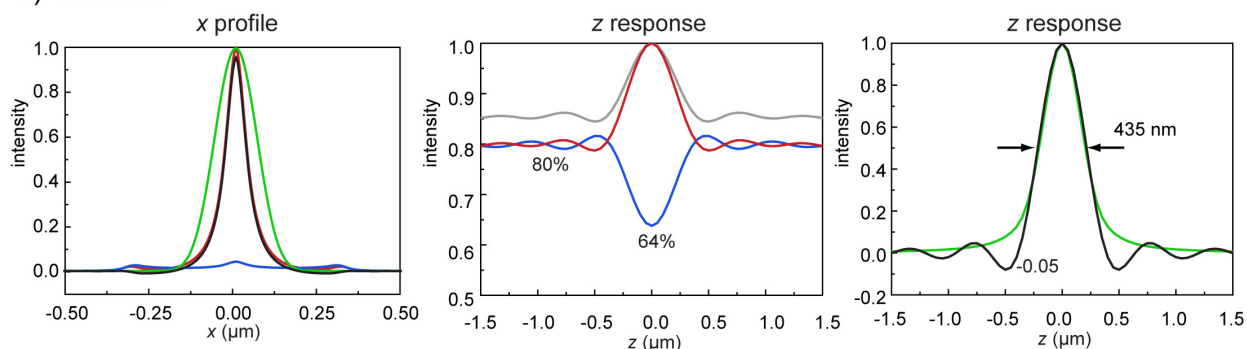
(b) Left column - detection probability distribution for a camera pixel at the center – the minimum of the off switching pattern (central detection). Right column – the average of four camera pixels centered on the surrounding peaks of the off switching pattern (peripheral detection). The scale bar of 200 nm applies to all images in the figure. The peripheral detection has been made four times brighter to utilize the full color scale.

(c) Effective detection probability I_c for a camera pixel at the center (left column), the average signal I_p of four pixels centered on the surrounding peaks of the off switching pattern (right column, brightness elevated by 10-fold) These probabilities display the contribution of a certain (x,y,z) coordinate in the focal region to the signal measured at the indicated (central or surrounding) camera pixel.

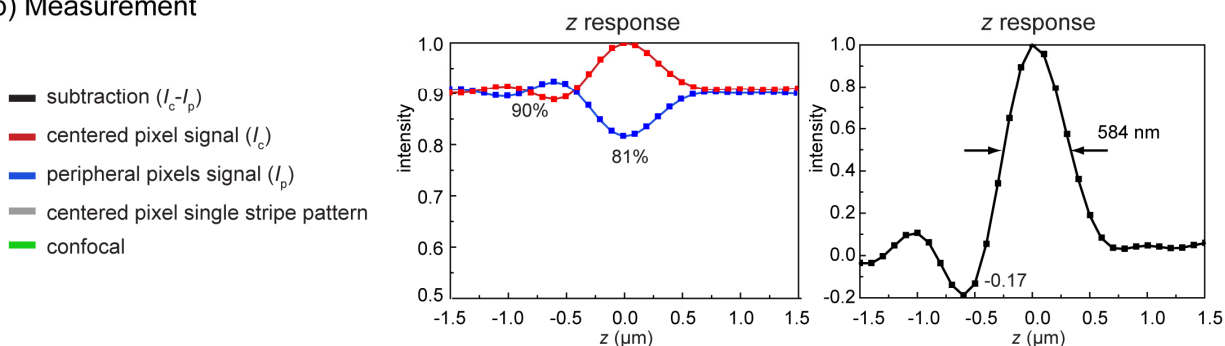
(d) Effective point-spread function (PSF) of our parallelized microscope after subtraction (left column) and an equivalent confocal version of our microscope. The improved lateral resolution of the subtraction data (over the confocal shown on the right panels) is not due to the subtraction but to the off switching of the proteins quantified in a.

Supplementary Figure 2: Calculation and measurement of the axial response of the microscope

a) Calculation



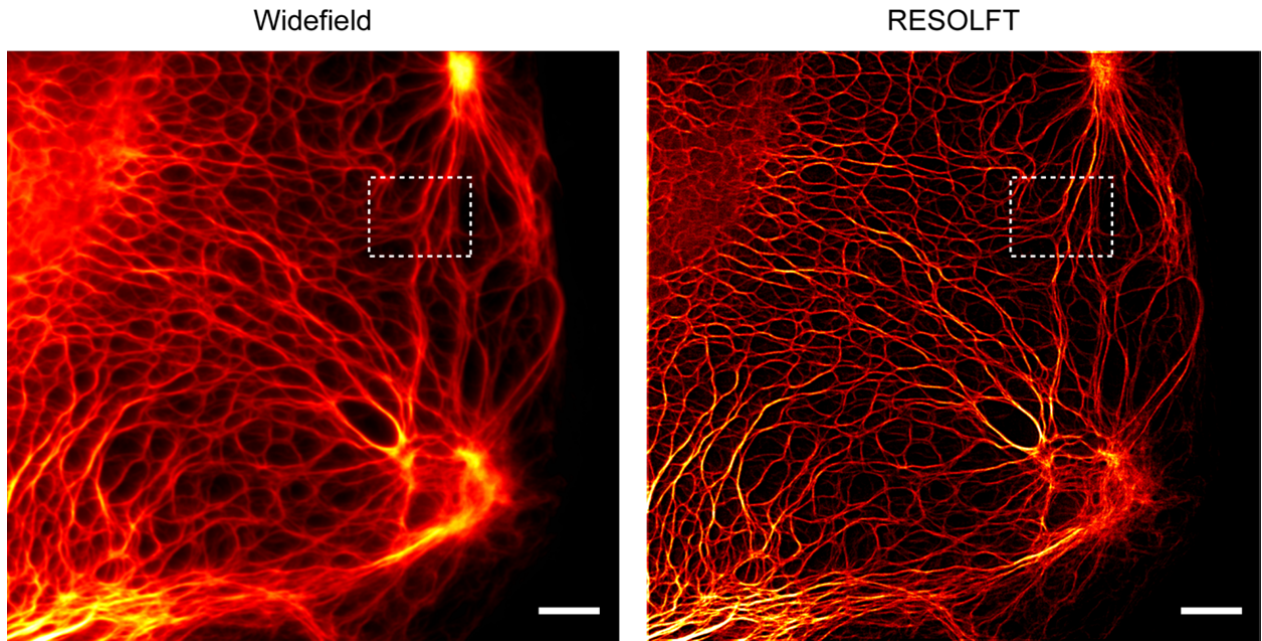
b) Measurement



(a) Profiles along the x axis for the effective PSFs shown in **Supplementary Fig. 1d** (left). Axial z responses calculated for the same PSFs by integrating over x and y . In gray: calculated z response as seen by a camera pixel at the center of a peak of the on-state distribution for an off switching pattern consisting of a standing wave in a single direction (producing stripes in the on-state distribution). The subtraction of central pixel and peripheral pixels signals and a z response for an equivalent confocal microscope (operating with the same aperture and excitation/emission wavelengths) are shown on the right.

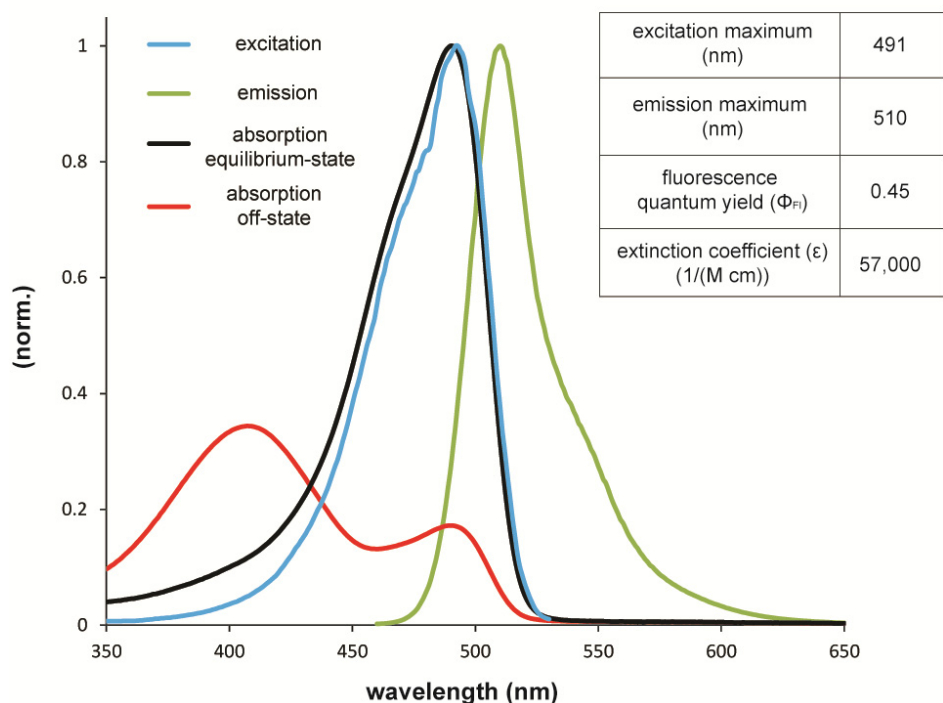
(b) Measurement of the z response of our parallelized microscope on a thin layer of rsEGFP(N205S) immobilized in polyamide acrylate (PAA) and corrected for photobleaching. The central and peripheral signals are shown on the left, the subtraction of both on the right.

Supplementary Figure 3: Full image of a section depicted in Fig. 2c-d



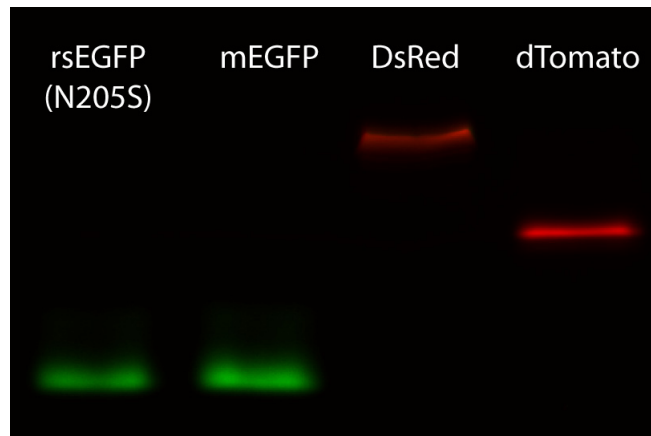
Living PtK2 cells expressing keratin19-rsEGFP(N205S) fusion protein. The white rectangle shows the area of **Fig. 2c-d**. Scale bar 5 μ m.

Supplementary Figure 4: Spectral properties of rsEGFP(N205S)



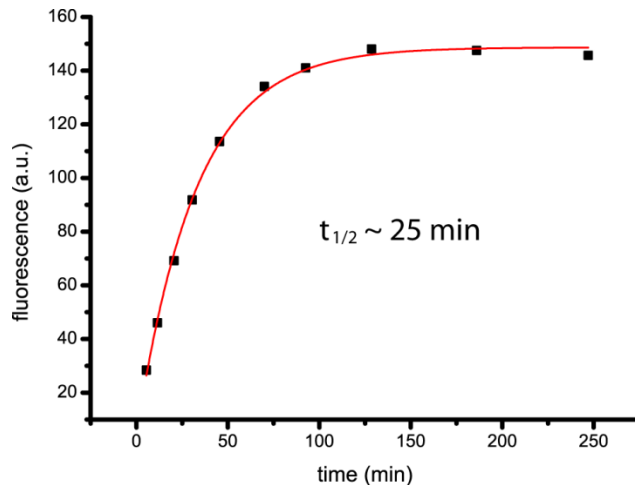
Normalized excitation (blue line) and emission (green) spectra. Normalized absorption spectra of the equilibrium- (black line) and off-state (red line). Excitation, emission, and absorption spectra were determined by measuring a protein solution of rsEGFP(N205S) at pH 7.5 with a fluorescence spectrometer (Varian Cary Eclipse, Varian) and a photospectrometer (Varian Cary 4000 UV/VIS, Varian). The emission spectrum was recorded by illuminating the protein solution with 450 nm light. The excitation spectrum was determined by detecting fluorescence at 560 nm. To determine the off-state absorption spectrum, the protein solution was illuminated with 480-520 nm light until no further changes in the absorption spectrum could be detected. Inset: key properties of rsEGFP(N205S). The molar extinction coefficient and the quantum yield of rsEGFP(N205S) were determined relative to the reported values of EGFP. (Patterson, et al. 1997)

Supplementary Figure 5: rsEGFP(N205S) is a monomer



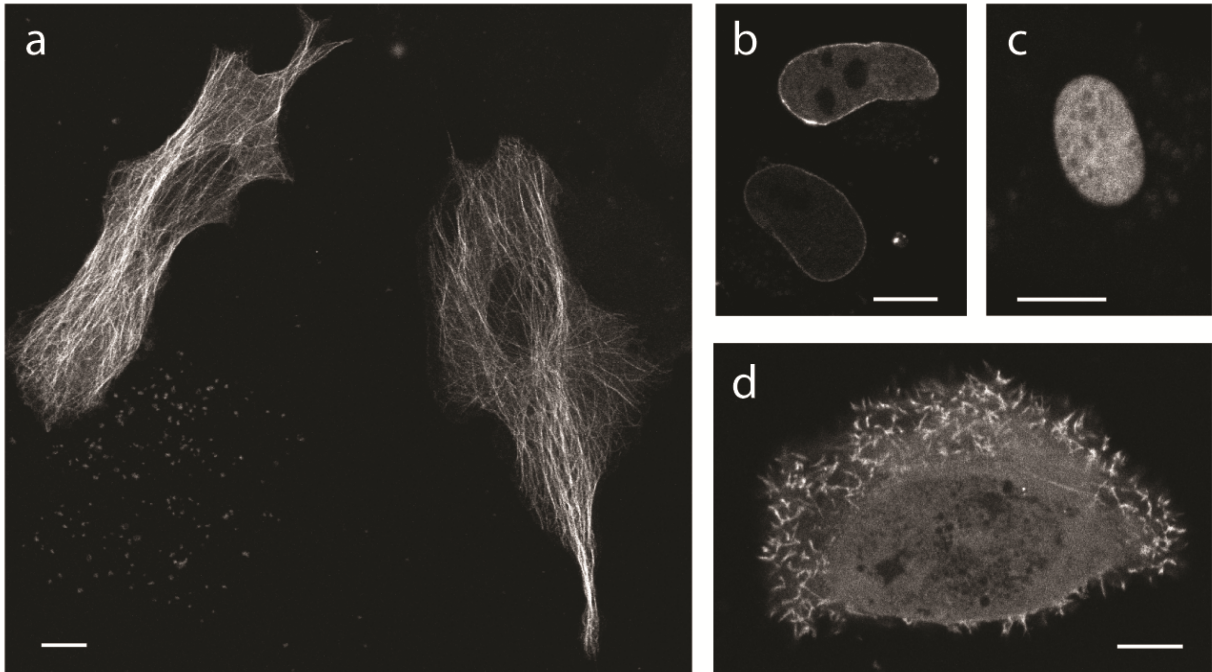
Purified rsEGFP(N205S), monomeric mEGFP, dimeric dTomato and tetrameric DsRed protein (1 μ g each) were separated on a semi-native PAGE gel and imaged as described previously (Grotjohann, et al. 2011)

Supplementary Figure 6: Maturation of rsEGFP(N205S) at 37 °C



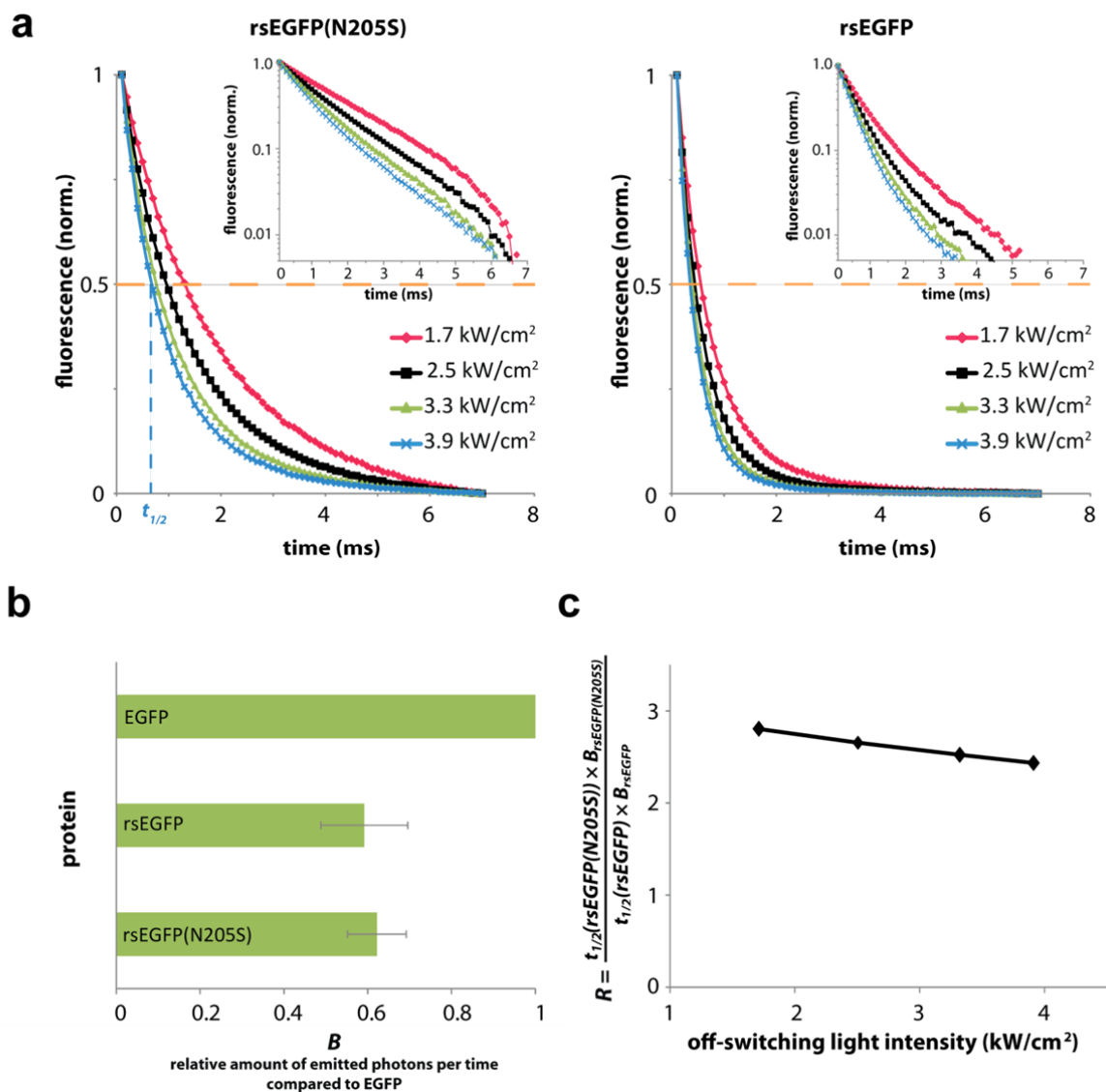
To determine the chromophore maturation time, the coding sequence of rsEGFP(N205S) was cloned into a pBad vector (Invitrogen) and transformed into TOP10 *E. coli* cells. An overnight culture was grown at 37 °C in LB-Amp medium. Subsequently, the overnight culture was used to inoculate 200 ml LB-Amp medium and incubated at 37 °C. Protein expression was induced by adding arabinose to a final concentration of 0.2 % when reaching an OD₆₀₀ of 0.5. After adding arabinose, the culture was placed in an air-tight container to reduce oxygen levels and agitated at 37 °C. After further incubation for three hours, the expressed protein was purified swiftly by NiNTA chromatography as described previously (Grotjohann, et al. 2011). To monitor the maturation of rsEGFP(N205S), fluorescence spectra were recorded at the indicated time points while incubating the protein solution at 37 °C.

Supplementary Figure 7: Expression of rsEGFP(N205S) fusion proteins in living mammalian cells



(a) rsEGFP(N205S)- α -tubulin, **(b)** Lamin B1-rsEGFP(N205S), **(c)** Histone H2B-rsEGFP(N205S), and **(d)** Vinculin-rsEGFP(N205S) expressed in Vero cells. Confocal images were recorded by combined irradiation with 488 nm and of 405 nm light; fluorescence was detected in the 495-550 nm range. The images represent single confocal sections. To generate the plasmid encoding the rsEGFP(N205S)- α -tubulin fusion, the coding sequence of rsEGFP(N205S) was amplified and cloned into the pEGFP-Tub plasmid (Clontech) replacing the EGFP sequence. To create plasmids coding for the fusion proteins shown in (b), (c) and (d), rsEGFP(N205S) was amplified and cloned into the gateway destination vector pMD-tdEosFP-N by replacing the tdEos coding sequence. The final expression plasmids were generated by gateway vector conversion as described previously. (Grotjohann, et al. 2011) Scale bar: 10 μ m.

Supplementary Figure 8: Switching kinetics and brightness of rsEGFP(N205S)

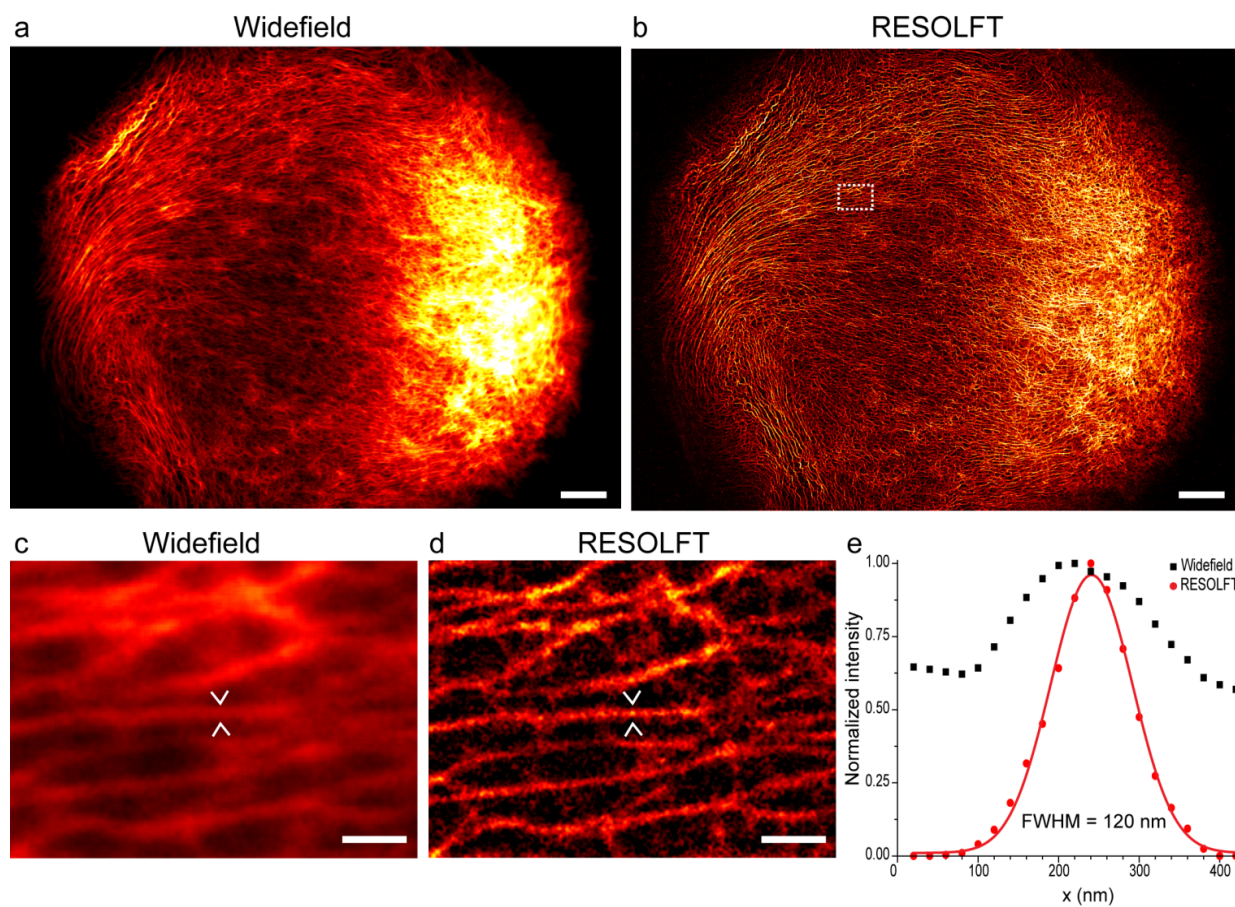


(a) Off-switching curves of rsEGFP(N205S) immobilized in polyamide acrylate (PAA) using various irradiation intensities. Switching was performed by irradiation at 488 nm after initial activation with 405 nm (0.5 kW cm^{-2} for 1 ms) light. The duration of activation with 405 nm light was chosen so that the proteins were fully activated. The curves were recorded with our microscope setup by reading out a small field of 240×16 pixels, permitting high acquisition frame rates (1,667 Hz). The camera exposure time was set to 100 μs . Laser exposure was triggered by the camera fire pulse.

(b) Fluorescence brightness determined from diffusing proteins in solution (buffer: 150 mM Tris, 100 mM NaCl; pH 7.5) using Fluorescence Intensity Distribution Analysis (FIDA) (Kask, et al. 1999)

(c) Increase in brightness of rsEGFP(N205S) over rsEGFP in terms of detected photons per cycle. The brightness is calculated as the brightness relative to EGFP (b) times the half decay times $t_{1/2}$ of the off-switching curves (a).

Supplementary Figure 9: Fast parallelized RESOLFT imaging with 120 μm x 100 μm field of view

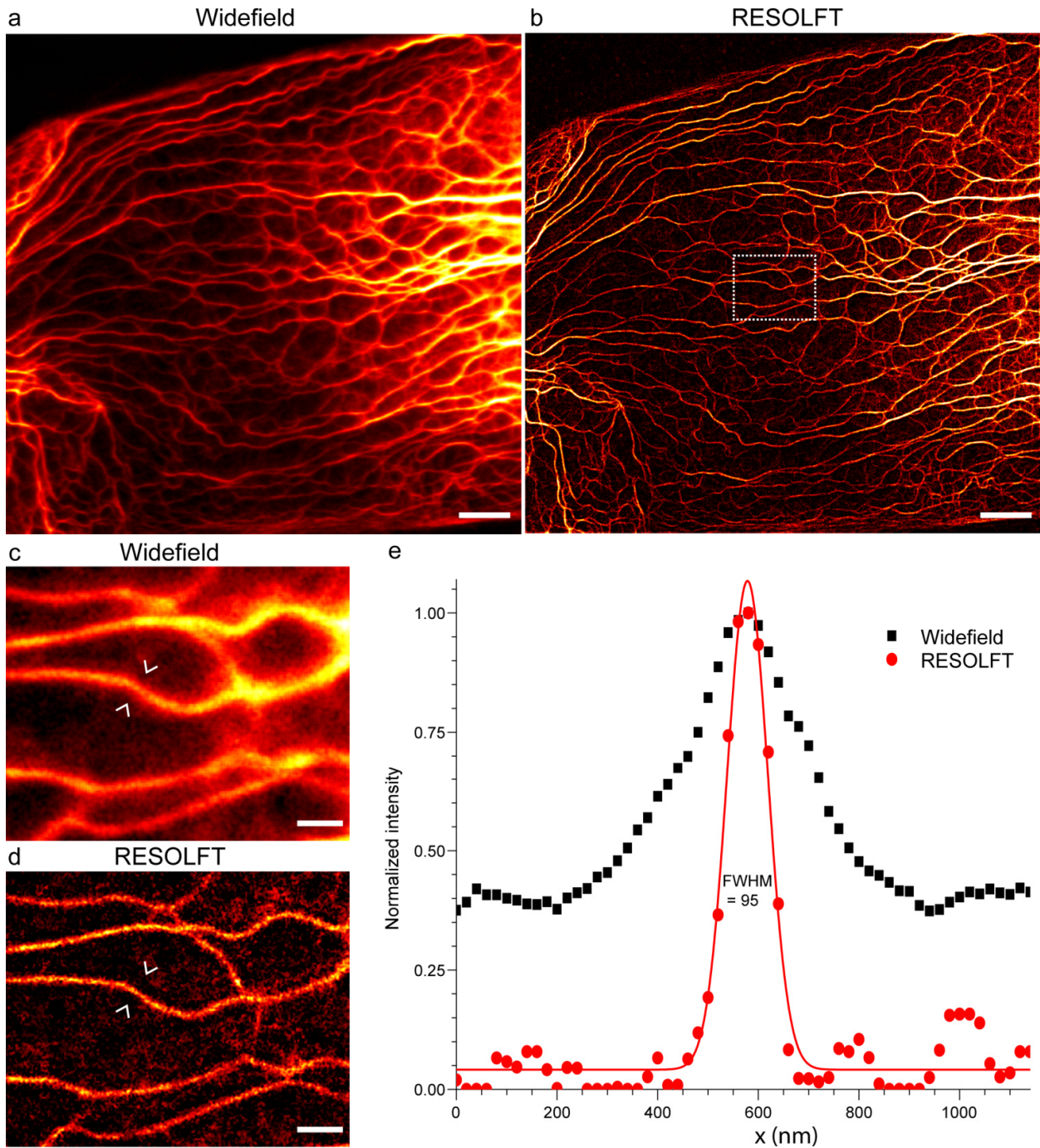


(a-b) Living PtK2 cells expressing keratin19-rsEGFP fusion protein. The image was reconstructed from 81 frames, each acquired in 12.6 ms. Total image acquisition time 1 s. Scale bar 10 μm .

(c-d) Widefield and RESOLFT magnification of a region in (a-b) of keratin19-rsEGFP in PtK2 cells. Scale bar 1 μm .

(e) Plot of normalized intensity profiles along the line marked with white arrows in c (black dots) and d (red dots). The latter profile is fitted to a Gaussian (red line) of 120 nm full-width-half-maximum (FWHM).

Supplementary Figure 10: Fast parallelized RESOLFT imaging with 50 μm x 50 μm field of view

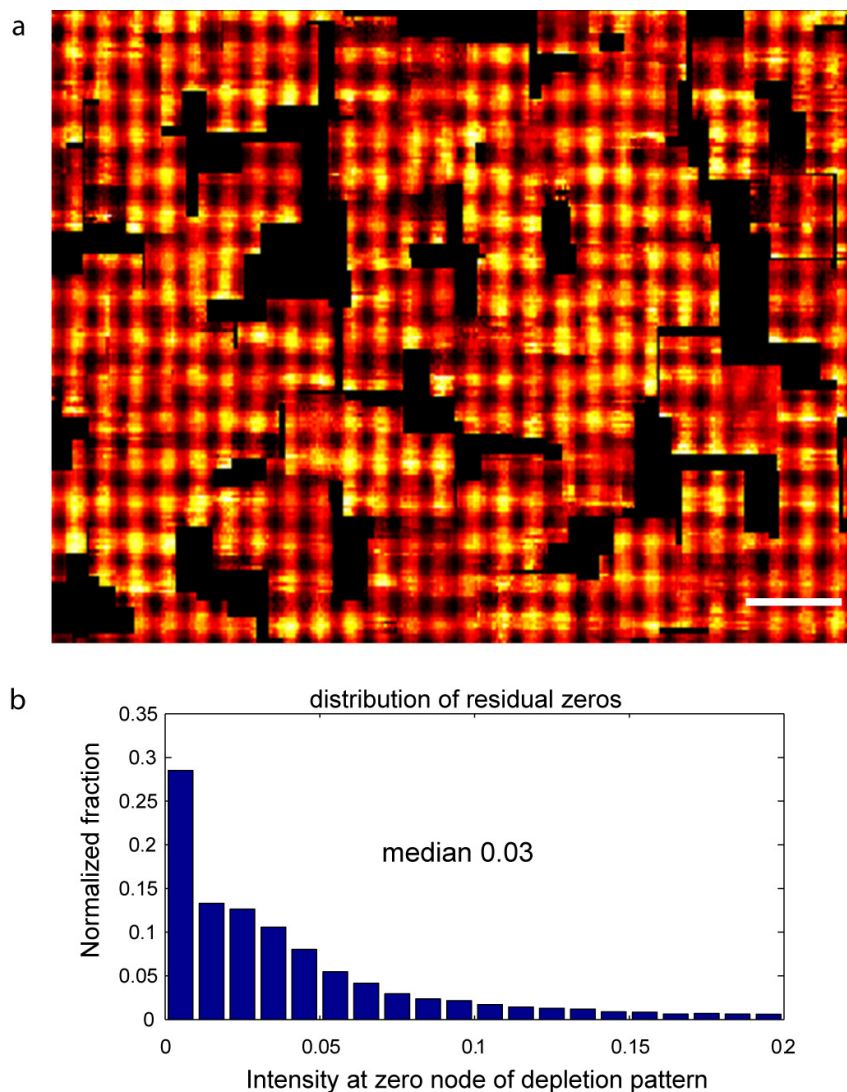


(a-b) Living PtK2 cells expressing keratin19-rsEGFP fusion protein. The image was reconstructed from 64 frames (scanning step 40 nm), each frame acquired in 6.25 ms. Total image acquisition time 0.4 s. Scale bar 10 μm .

(c-d) Wide field and RESOLFT magnification of a region in (a-b) of keratin19-rsEGFP in PtK2 cells. Scale bar 1 μm .

(e) Plot of normalized intensity profiles along line marked with white arrows in c (black dots) and d (red dots) images. The later profile is fitted to a Gaussians (red line). Gaussian width is 95 nm.

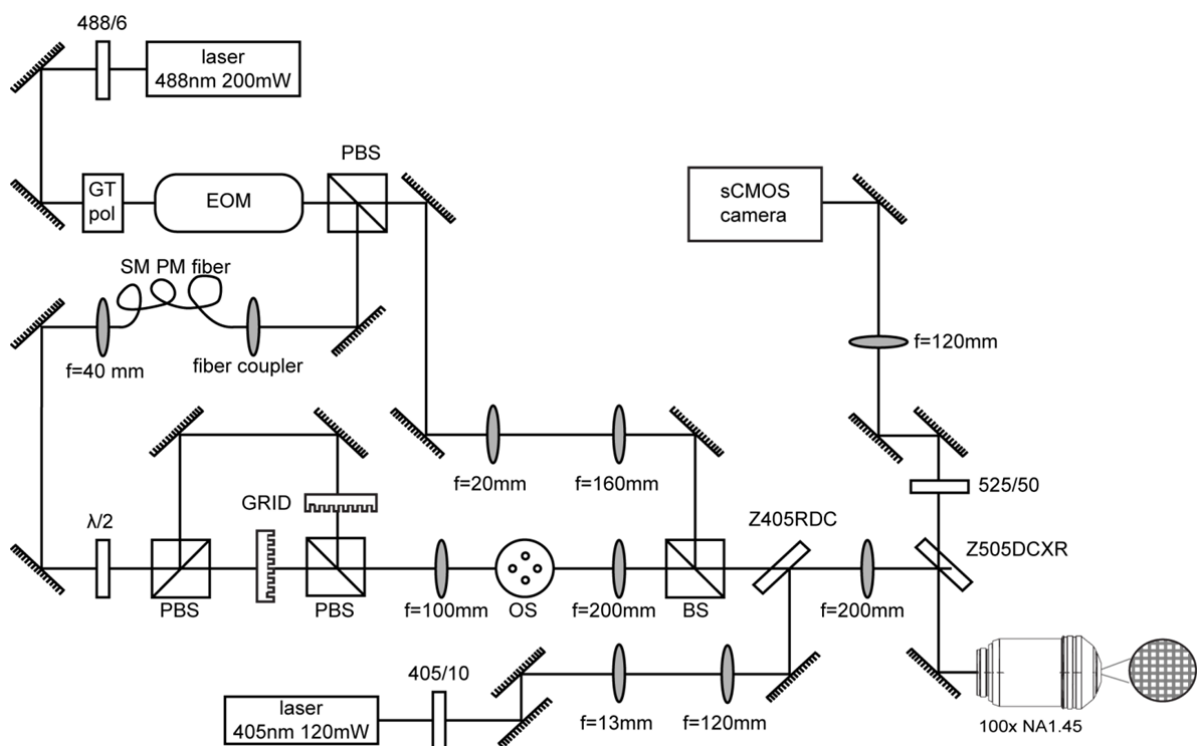
Supplementary Figure 11: Off-switching (deactivation) pattern in parallelized RESOLFT



(a) Representative fraction of our off-switching pattern measured by scanning multiple but isolated fluorescent beads of 40 nm in diameter across the focal plane. Each bead was scanned about 2 pattern periods p in each direction. The average bead position and the amplitude of the detection PSF (assumed Gaussian), plus a locally constant background were fitted in each camera frame. The resulting amplitudes and bead positions probe the local deactivation pattern with an accuracy that is given by the bead diameter. The image consists of data gained from measurements on 5 different bead configurations. To minimize mismatch, regions with overlapping measurements from several beads are combined by suitable scaling of the initial bead brightness. Large sections of the deactivation pattern can be probed and large connected areas of the pattern appear. Estimates of the depth of the ‘zeros’ in the pattern (contrast ratio between minimum and surrounding peak) can be given by dividing each local minimum by the average of the surrounding maxima.

(b) The median value of all estimated values for the remaining intensity of the zero position is 3%.

Supplementary Figure 12: Detailed diagram of the parallelized RESOLFT microscope



488/6	Excitation clean-up filter	Semrock, USA
GT pol	Glan-Thomson polarizer	B. Halle Nachfl., Germany
EOM	Electro optical modulator (LINOS LM0202P5W)	Qioptiq, Germany
PBS	Polarizing beam splitter cube	B. Halle Nachfl., Germany
fiber coupler	Coupler 60FC-4-4.5S-01	Schäfter+Kirchhoff, Germany
SM PM fiber	Single mode polarization maintaining PC/APC fiber P5-488PM-FC-2	Thorlabs, USA
$\lambda/2$	Half wave plate polarization retarder	B. Halle Nachfl., Germany
GRID	Phase diffraction gratings with period 36 μm and height 437 nm SiO_2	Laser-Laboratorium Göttingen, Germany
OS	Order selection mask made of cardboard with 4 holes	
BS	50:50 beam splitter cube	Newport, USA
Z405RDC	Dichroic mirror on 6 mm thick substrate	Chroma, USA
505DCXR	Dichroic mirror on 6 mm thick substrate	Chroma, USA
525/50	Fluorescence filter HC525/50	Semrock, USA
405/10	Excitation clean-up filter	Semrock, USA

Supplementary note 1: Lateral on-state spatial distribution

Here we derive an expression of the distribution of the fluorophore on-state after application of the off switching pattern in our parallelized RESOLFT microscope. The off switching pattern is approximated by a sum of two orthogonal sinusoidal functions:

$$I_{\text{Off}}(x, y) = \sin^2\left(\frac{\pi x}{l}\right) + \sin^2\left(\frac{\pi y}{l}\right) \quad (1)$$

where l is the period of the pattern, x and y are spatial coordinates. With all fluorophores uniformly being switched on (activation) before switching off (deactivation), the distribution of the remaining fluorophores in the on-state is (Hell 2003):

$$D_{\text{act}}(x, y) = \frac{1}{1 + \zeta I_{\text{Off}}(x, y)} = \frac{1}{1 + \zeta \left[\sin^2\left(\frac{\pi x}{l}\right) + \sin^2\left(\frac{\pi y}{l}\right) \right]} \quad (2)$$

where $\zeta = I/I_s$ is defined as the saturation factor. I denotes the peak intensity of the sinusoidal pattern and I_s is the intensity at which the on-state population is reduced to 50%.

Eq. (2) approaches a rotationally symmetric shape for large ζ . This follows from a Taylor series expansion, first derived for variable x :

$$D_{\text{act}}(x, y) = \frac{1}{1 + \zeta \left[\sin^2\left(\frac{\pi x}{l}\right) + \sin^2\left(\frac{\pi y}{l}\right) \right]} = \frac{1}{1 + \zeta \sin^2\left(\frac{\pi x}{l}\right)} - \frac{\zeta \pi^2}{\left[1 + \zeta \sin^2\left(\frac{\pi y}{l}\right)\right]^2 l^2} x^2 + \text{Order}(x^4) \quad (3)$$

The series can be restricted up to the 2nd order, because at reasonably high ζ this distribution is non-zero for small coordinates only, where higher orders are negligible. Another Taylor series expansion in Eq. (3) for coordinate y yields:

$$D_{\text{act}}(x, y) \approx 1 - \frac{\zeta \pi^2}{l^2} x^2 - \frac{\zeta \pi^2}{l^2} y^2 + \frac{2\zeta^2 \pi^4}{l^4} x^2 y^2 + \text{Order}(y^4) \quad (4)$$

Again, we can neglect higher orders in y as well as cross terms $x^2 y^2$. Thus, we obtain in the limit of large ζ :

$$D_{\text{act}}(x, y) \approx 1 - \zeta \omega^2 x^2 - \zeta \omega^2 y^2 = 1 - \zeta \omega^2 r^2 \quad (5)$$

where $\omega = \pi/l$ is the radial frequency of the pattern, and r is a radial coordinate (distance from a zero of the off switching pattern). The rotational symmetry of the on-state around each zero position of the off switching (deactivation) pattern becomes obvious.

The full width at half maximum (FWHM) Δr of the peaks around each zero position of the off switching pattern can be easily computed by solving Eq. (5) for values r where the value of D_{act} equals to 1/2:

$$\Delta r = \frac{\sqrt{2} l}{\pi} \frac{1}{\sqrt{\zeta}} \quad (6)$$

Expression (6) is well-known in RESOLFT and STED microscopy (Hell 2003) and depicts the inverse square root dependence of resolution (FWHM) on the saturation factor ζ , which is multiplied by $\sqrt{2}$ because of the superposition of two beams in the deactivation pattern. Also, it demonstrates that for our parallelized RESOLFT setup with the incoherently crossed standing wave pattern, the achievable FWHM is proportional to the period of the sinusoidal pattern. Smaller periods will result in smaller FWHMs and consequently in higher resolution. However, if the period is too small (at the diffraction limit of imaging the on-state fluorophores to the camera), there will be significant cross-talk between the signal originating from neighboring zeros (Gustafsson 2005).

To assure the range ζ where the approximation in Eq. (5) holds, numerical calculations using MATLAB were performed. They show good correspondence for saturation levels of 5 and higher; see 2D intensity maps in **Fig. 1c**.

Supplementary note 2: Optical sectioning capability of the parallelized microscope

It is known that widefield microscopes using ‘structured illumination’ can display optical sectioning comparable to that of a confocal microscope (Karadaglic and Wilson 2008). We present a theoretical analysis and experimental results that quantify the axial resolution of our parallelization scheme.

First the detection point-spread-function for camera pixels centered on a peak of the effective on-state distribution were calculated. Since the sample is shifted during scanning, the position of the camera pixels remains unchanged with regard to the position of the on-state peaks. However, not all peaks have the camera pixels centered on them. The interpolation required to obtain the signal at the position of the peaks is equivalent to using centered pixels that are somewhat larger, but for the analysis here we neglect this effect.

The effective PSF of the imaging system is the product of the effective on-state distribution and the detection PSF because the excitation for readout is carried out with uniform illumination and does not affect the resolution. The effective on-state distribution has already been derived in **Supplementary Note 1**, Eq. (2). For our large field of view (of $> 100 \mu\text{m}$ diameter) no significant axial dependence is present in the off-switching pattern. Therefore, we can adopt Eq. (2) directly for the 3D on-state distribution.

In **Supplementary Fig. 1** the on-state distribution as well as the normalized detection sensitivity for ‘on-peak’ and ‘off-peak’ pixels, and the effective PSF of the imaging system are shown. The subtraction of the signals for a camera pixel centered on a peak of the on-state distribution and the average signal of four camera pixels surrounding the same peak gives the effective PSF describing the imaging properties of our setup. The lateral width of the effective PSF is almost identical with the width of the peaks in the on-state ($\sim 80 \text{ nm}$) while the value for the axial width is between the confocal and the wide field (detection only) case, because of the subtraction. The minimal on-state population amounts to about 6% of its maxima and is located at the maxima of the off switching pattern.

Axial resolution is often quantified by the response to an ultrathin lateral (xy) layer, i.e. the z response. It can be calculated by integrating the effective PSF in x and y . A pure widefield PSF, for example the ‘on-peak’ pixel readout PSF, does not display any discrimination in the z -direction (i.e. the z response is constant). However, its multiplication with the on-state distribution exhibits a modulation (red curve in the central plot in **Supplementary Fig. 2a**). The background can be suppressed by subtracting the averaged ‘off peak’ signal. The final signal is a z response featuring a width similar to its confocal counterpart and negative overshooting artifacts of less than 5% of the maximum value. A 1-dimensional off-switching pattern exhibiting a pattern of stripes of on-state molecules requires subtraction of a larger background ($\sim 85\%$).

We also measured the z response on a protein layer and verified the optical sectioning property of the parallelized microscope. (**Supplementary Fig. 2b**) Background and width of the subtracted signal are slightly larger than calculated. We attribute this to optical imperfections of the setup, particularly to spherical aberrations.

Supplementary note 3: Flat field correction of the sCMOS camera

For count rates <1000 counts per pixel and fast read-out as well as high gain we frequently see distinct variations in sensitivity of some (~1%) of the pixels, i.e. these pixels under- or overestimate the true incident illumination significantly. Many state-of-the-art sCMOS cameras seem to suffer from this non-uniform sensitivity. In our case, the affected pixels are either still linearly mapping the incoming light intensity (but with a lower rising factor), or they seem not to gain sufficient counts in the <100 counts regime, and also not catching up later. While some of these pixels seem to constantly show this behavior, we also observed daily changes for others.

As our imaging scheme depends on single-pixel information, we repeatedly employed a calibration routine: We illuminated the camera area homogeneously with a dimmable ordinary lamp with variable brightness, as in typical fluorescence conditions. For each count rate we recorded a large number (~1000) of identically bright images and added them up to eliminate readout noise. In the add-up, the erroneous pixels can clearly be identified. A smoothed (10 pixel width) add-up estimates the true (average) pixel values. Dividing it by single pixel values of the add-up gives a calibration for each pixel. Using linear interpolation we can adapt this calibration to intermediate brightness levels. This correction was applied to all raw data frames before further processing.

References for Supplementary Material

- 1 Patterson, G. H., Knobel, S. M., Sharif, W. D., Kain, S. R. & Piston, D. W. Use of the green fluorescent protein and its mutants in quantitative fluorescence microscopy. *Biophysical Journal* **73**, 2782-2790 (1997).
- 2 Grotjohann, T. *et al.* Diffraction-unlimited all-optical imaging and writing with a photochromic GFP. *Nature* **478**, 204-208, doi:10.1038/nature10497 (2011).
- 3 Kask, P., Palo, K., Ullmann, D. & Gall, K. Fluorescence-intensity distribution analysis and its application in biomolecular detection technology. *Proceedings of the National Academy of Sciences of the United States of America* **96**, 13756-13761 (1999).
- 4 Hell, S. W. Toward fluorescence nanoscopy. *Nature Biotechnology* **21**, 1347-1355 (2003).
- 5 Gustafsson, M. G. L. Nonlinear structured-illumination microscopy: Wide-field fluorescence imaging with theoretically unlimited resolution. *Proceedings of the National Academy of Sciences of the United States of America* **102**, 13081-13086 (2005).
- 6 Karadagic, D. & Wilson, T. Image formation in structured illumination wide-field fluorescence microscopy. *Micron* **39**, 808-818, doi:10.1016/j.micron.2008.01.017 (2008).